RSC Advances

PAPER

View Article Online
View Journal | View Issue

Cite this: *RSC Adv.*, 2020, **10**, 11716

Enteric pH responsive cargo release from PDA and PEG coated mesoporous silica nanoparticles: a comparative study in *Drosophila melanogaster*†

Nidhi Sapre, ‡[a] Rusha Chakraborty, ‡[b] Poorvi Purohit,[c] Suresh Bhat,[c] Gaurav Das *[b] and Sneha R. Bajpe *[a]

Received 30th December 2019
Accepted 13th March 2020

DOI: 10.1039/c9ra11019d

rsc.li/rsc-advances

Physiological stimulus-specific cargo release from nanoparticle carriers is a holy grail of drug delivery research. While the majority of such work is carried out *in vitro* with cell lines, widespread use of common mammalian model systems – mice and rats – is difficult due to the associated cost and regulatory restrictions. Here we use the inexpensive, easily reared, excellent genetic model system *Drosophila melanogaster* to test pH responsive cargo release from widely used mesoporous silica nanoparticles (MSNs) coated with pH sensitive polydopamine (PDA) and polyethylene glycol (PEG) polymers. We synthesized 650 ± 75 nm diameter PDA or PEG coated mesoporous silica nanoparticles loaded with a fluorescent dye and fed to individual adult flies. Subsequently, the passage of the particles were monitored through the fly gut. As in mammals, the fly intestine has multiple pH specific zones that are easily accessible for imaging and also genetic, biochemical or physiological manipulations. We observed that both the species of MSNs ruptured around the acidic (pH < 4.0) middle midgut of the flies. PEG coated particles showed sharper specificity of release in the acidic middle midgut of flies than the PDA coated ones and had less tendency to clump together. Our results clearly show that the *Drosophila* gut can be used as a model to test pH responsive biocompatible materials *in vivo*. Our work paves the way for greater use of *Drosophila* as an *in vivo* complete systemic model in drug delivery and smart materials research. It also suggests that such specific delivery of chemical/biological cargo can be exploited to study basic biology of the gut cells and their communication with other organs.

1 Introduction

Maintaining tight control over the amount of drug released as-and-when needed by the human body is a long-standing challenge for drug delivery research.[1] Functional materials such as zeolites,[2,3] metal–organic frameworks,[4–7] zeolitic imidazole frameworks[8,9] *etc.*, are some of the most popular class of materials used in drug delivery research.[10] These materials, due to their biocompatibility and high porosity can be used as effective drug carriers. Among the various nano-sized carrier materials studied for drug delivery, mesoporous silica is perhaps the most popular due to its easy synthesis, high porosity and stability.[11–16] Mesoporous silica nanoparticles (MSNs) are porous solids with a large number of honeycomb-like pores that can accommodate a wide variety of cargo molecules. These biocompatible materials have large surface area (>900 $m^2\ g^{-1}$), large pore volume (>0.9 $cm^3\ g^{-1}$) and tunable pore size (2–10 nm).[16] Despite the established biocompatibility,[18] non-functionalized MSNs lack the ability to specifically and efficiently react to external physiological stimuli and could disintegrate leading to premature cargo-release.[18–20] Temporal or location specific cargo-release can be enhanced by (i) introducing additional molecular gates[17,19] into the silica matrix that open on receiving stimuli such as changes in pH,[20] redox,[21] temperature[17] *etc.*, or (ii) by coating the silica nanoparticles with a stimulus responsive polymer.[12,20,22–24] As an example, change in pH during cellular endocytosis can cause disintegration of responsive polymers surrounding carrier nanoparticles to release their cargo in a controlled manner.[18,20,25,26] Among the various polymers used, polyethylene glycol (PEG)[24,27–30] is popular due to its biocompatibility and biodegradability.[26,31] One other polymer used frequently in nanomaterial coating is polydopamine (PDA);[23,32–37] a polymeric oxidation product of the catecholaminergic neurotransmitter dopamine. It has a molecular structure similar to that of the naturally occurring pigment melanin (eumelanin) and possesses the ability to be deposited on all types of inorganic, organic and superhydrophobic surfaces.[32,38] *In vivo* testing of

[a]*Symbiosis Centre for Nanoscience and Nanotechnology, Symbiosis International (Deemed University) (SIU), Pune, India. E-mail: sneha.bajpe@scnn.edu.in*

[b]*National Centre for Cell Science, Pune, India. E-mail: gauravdas@nccs.res.in*

[c]*CSIR-National Chemical Laboratory, Pune, India*

† Electronic supplementary information (ESI) available. See DOI: 10.1039/c9ra11019d

‡ Equal contribution first author.

functional drug-delivering materials in a biological system is critical to ascertain its suitability for biological applications. Usually, such testing of new materials and drugs are carried out in animal or human derived cell lines.[39–42] While this approach has been helpful, the effect of these molecules in context of a complete organism with distinct organs and a holistic, systemic milieu cannot be modeled with cell lines.

The fruit fly or vinegar fly *Drosophila melanogaster*, is a versatile genetic model that can be grown easily and inexpensively and offer a well-developed genetic tool kit to manipulate all its genes, cell types, tissues and organs.[43–45] Importantly, flies and humans have homologous genes and organs, making it possible to model human diseases and study their underlying genetic, cellular and physiological mechanisms.[46–50] For the same reasons flies also lend themselves for rapid testing of materials, including nanomaterials or nanoparticles, for their toxicity, biocompatibility and mode of action.[51–59] However, there has almost been no effort to use flies for *in vivo* screening of smart carrier materials and stimulus responsive drug release.[58,60] The fly gut bear remarkable similarity with the human gut.[61] Both have similar developmental origin, harbour stem cells in its luminal epithelial lining, have neuronal innervations and secrete digestive enzymes in distinct zones that break down nutrients and facilitate their absorption through the gut epithelium. Importantly, like the mammalian gut, the fly gut has distinct pH zones that range from highly acidic in the middle midgut (pH < 4) to neutral in the foregut, crop & anterior midgut (pH ~ 7.4) and to alkaline (pH ~ 9–11) in the posterior midgut & hindgut.[62–64] Here, we hypothesized that we can utilize the fly gut pH microenvironments to test zone-specific cargo release from smart carrier materials. We report a comparative study of cargo release from fluorescent dye loaded MSNs coated with two pH responsive polymers, PDA and PEG in the *Drosophila* gut. Our results indicate that both these particles readily release their cargo in the middle midgut (MMG) acidic zone and are not toxic to flies. Our studies poise the *Drosophila melanogaster* gut as an accessible model to screen pH stimulus specific cargo release in a well characterised genetic model organism.

2 Experimental section

2.1 Chemicals

Tetraethyl orthosilicate (TEOS) (cat. no. 8.00658), hexadecyl trimethyl ammonium bromide (CTAB) (cat. no. 8.14119), PEG400 (cat. no. 8.07485), hydrochloric acid (cat. no. 1.93401.0521) were purchased from Merck, India. Ammonia solution (cat. no. 78719) was purchased from SRL Chemicals, India. Potassium hydroxide (cat. no. Q26705) was purchased from Qualigens, India. Dopamine hydrochloride (cat. no. H8502) and bromothymol blue (cat. no. 114413) was purchased from Sigma Aldrich, India. Rhodamine B (cat. no. GRM980) was purchased from Hi-Media, India. Ethanol (cat. no. 32221) was purchased from Honeywell, India. Amaranth FCF food grade dye was purchased from Vidhi, Pune, India (batch no. PAM13568). Agarose (cat. no. 180720), low melting agarose (cat. no. AGAL0050) and PBS tablets (cat. no. 2810301) were purchased from MP Biomedicals, India. All chemicals were used without further purification. Milli-Q® and RO water were used for all experiments.

2.2 Synthesis

2.2.1 Synthesis of mesoporous silica nanoparticles (as-synthesized MSN). MSNs were synthesized by standard sol–gel process.[15,65] 1.6 g of CTAB was dissolved in 35% [w/v] ethanol : water solution containing 10 mL of ammonia (10 mL, 25 wt%). This reaction mixture was heated at 35 °C, and 10 mL TEOS was added rapidly under vigorous stirring. The reaction mixture was stirred for 24 h. The reaction product was collected by vacuum filtration and washed thrice with 35% ethanol : -water and dried at 60 °C under vacuum, overnight. The white powder was then dispersed in acidified ethanol (400 μL of concentrated HCL in 200 mL of ethanol) and stirred at 30 °C for 2 h. This step was repeated thrice for removal of template and then the sample was washed three to four times with water and dried at 60 °C under vacuum, overnight.

2.2.2 Loading MSNs with rhodamine B (RhB) – uncoated RhB@MSN. A solution of 5 mg of RhB in 100 mL of water was used for loading the MSNs. The synthesized MSNs were dispersed in the RhB solution by sonication for 5–10 minutes and kept in a rotating mixer for 24 h. The sample was then washed three times with water and centrifuged after every wash for 10 minutes at 4000 rpm at 25 °C. The pink colored product was dried at 40 °C under vacuum, overnight.

2.2.3 Surface coating of rhodamine B (RhB)-loaded MSNs

2.2.3.1 PEG coated RhB@MSN. 1 g of RhB@MSNs were added to 100 mL of water and sonicated for 5–10 minutes. After sonication, 10% of PEG-400 was added to this solution and the whole mixture was stirred for six hours. The mixture was then washed several times with water, followed by centrifugation at 4000 rpm at 25 °C for 10 minutes. The final product was collected and dried in a desiccator.

2.2.3.2 PDA coated RhB@MSN. 1 g of RhB@MSNs were added to Tris–HCL buffer (10 mM, pH 8.5) containing dopamine hydrochloride (500 mg of dopamine in 500 mL) and sonicated for 5–10 minutes. The mixture was then stirred for six hours. The mixture was then washed several times with water, followed by centrifugation at 4000 rpm at 25 °C for 10 minutes. The final greyish black product was collected and dried at 40 °C under vacuum, overnight.

2.3 Physicochemical characterization

Dynamic light scattering (DLS) & zeta potential measurements were performed on Anton Paar Litesizer 500, Anton Paar, GmbH. The samples were measured for 1 min and auto fitting of the correlation function was performed using the Anton Paar DLS software Kalliope. Zeta potential measurements were performed using an Omega cuvette. Scanning electron microscopy (SEM) was performed on Carl Zeiss EVO 18, Zeiss, USA. The powder samples were gold sputtered before measurement. Transmission Electron Microscopy (TEM) was performed on Philips CM200; operating voltage: 20–200 kV, resolution: 2.4 Å. The samples were suspended in water and loaded on a Cu grid

and air dried before measurement. X-ray photoelectron spectroscopy (XPS) measurements were performed using K-Alpha + XPS instrument, Thermo Fisher, UK, with Al Kα (monochromatic) using 6 mA beam current at 12 kV. The instrument was calibrated with Ag 3d 352 eV. The samples were drop casted on a silicon wafer and mounted on a standard SS plate with conductive carbon tape and loaded into the sample chamber with a vacuum pressure of 1.2×10^{-8} mbar. Sample spot size was 400 μm and the reference binding energy was C 1s (284.8 eV). Brunauer–Emmett–Teller (BET) surface area analysis by Nitrogen adsorption and desorption were carried out using Quadrasorb SI, Quantachrome Instruments, Anton Paar, GmbH. Pore size distributions were calculated from adsorption isotherm using the BJH method. Fourier transform infrared (FTIR) measurements were performed on a PerkinElmer Spectrum-GX, PerkinElmer, USA, at resolution 4 (nm $Å^{-1}$), scan range from 4000–600 cm^{-1}, the total number of scans 16 and samples were scanned directly in ATR mode. All graphs were plotted using Igor Pro software, Wavemetrics, USA. Confocal microscopy images for the synthesised nanoparticles were obtained on a Zeiss LSM 880 confocal microscope, Zeiss, USA. 1 : 10 dilutions of 1 mg mL^{-1} PEG/PDA coated RhB@MSN samples were prepared in 1% low melting (LM) agarose (MP Biomedicals, cat. no. AGAL0050) and 20 μL of each solution was added on a clean glass slide. The added droplets were immediately covered with a coverslip and allowed to spread. Coverslips were sealed with transparent nail polish and imaged with Airyscan 2.0 scanner using 40× (plan-apochromat/1.4 oil DIC M27) and 100× (α plan-apochromat/1.46 oil DIC M27 Elyra) objectives. pH of various solutions were checked using Hanna (HI-5521-02) pH meter, Hanna Instruments, USA.

2.4 *In vitro* RhB release studies

Three different pH solutions were prepared: starting with 1 mM HCl (pH 3.0) and then adjusting pH by the addition of 1 mM KOH to obtain solutions of pH – 7.4 and 9.0. 5 mg of samples were weighed separately in different vials to which 2 mL of different pH solutions were added and the vials were rotated using a rotating mixer for different time periods (between 0 to 5 h). All samples were then centrifuged at 4000 rpm for 10 minutes at 25 °C and absorbance measurements were performed on the supernatants at 553 nm wavelength. The blank was subtracted from each measurement. The measurements were repeated thrice per sample and the samples were measured in duplicates.

2.5 Fly experiments

2.5.1 pH profile of *Drosophila* gut. To visualize the pH zones of an adult fly gut generally, a pH indicator dye is fed along with the food and dissected guts are then imaged under a microscope.[62–64] We followed a similar procedure using 0.1% of the pH indicator dye bromothymol blue with standard fly cornmeal food medium and poured into fresh vials. After the food media solidified and cooled down, 0 to 4 days old adult females that were food starved for the previous 24 hours were transferred into the vials and allowed to feed for 2 hours at 25 °C and ∼60% humidity. Flies were subsequently anesthetized in 70% ethanol for 30 seconds and dissected using a pair of fine forceps (#5 cat. no. 11295-10 and #55 cat. no. 11295-51, Dumostar, FST). Guts were washed 2–3 times using ice cold PBS (1×). A drop of mounting media was placed on a clean microscope glass slide (75 mm × 25 mm × 1.35 mm, Bluestar) and evenly spread using a 20 μL pipette tip. After dissection, the fly gut was placed in the mounting media and arranged carefully for clear identification of each part of the gut during imaging. Image of the whole gut was captured using a mobile phone camera through a stereo microscope (Nikon SMZ445) with 3.5× zoom.

2.5.2 *In vivo* release studies on *Drosophila*

2.5.2.1 Feeding. To deprive flies of food and water, 25–30 females were transferred to an empty vial with dry filter paper and kept in an incubator at 25 °C and ∼60% humidity for 12–14 hours. Resultant hungry and thirsty flies were then transferred to a fresh empty vial. The flies were ice anesthetized and 10–15 healthy flies were immobilized on a glass slide using nail polish with their wings stuck on the surface of the glass slide with their abdomens facing up (see ESI Fig. SI-8†). Flies were allowed to recover for 30 minutes at 25 °C. A 1 μL droplet of 0.1 mg mL^{-1} of PEG coated and 0.02 mg mL^{-1} of PDA coated RhB@MSN solution in RO water (adjusted to pH 7.0) were fed to individual flies using a 0.1–3 μL micro pipette for 10 seconds. Only flies that fed continuously for ∼10 seconds were used for further experimentation. Subsequent to feeding, flies on the glass slide were placed in a petri dish with a wet filter paper at the bottom to avoid dehydration and kept at 25 °C for 30 min.

2.5.2.2 Dissection and mounting. Nanoparticle fed flies were transferred to a vial containing 70% ethanol for 30 seconds and anesthetized. After anesthetization, their guts were dissected and washed 2–3 times with 1× PBS before mounting as described above. No more than 2 guts were mounted between two glass cover-slip (18 mm × 18 mm × 1 mm, Bluestar) spacers were glued with nail polish ∼10 mm apart onto the slide and a third cover-slip was carefully placed over the sample. Mounting media was added gently from one of the open edges and allowed to wick completely to just submerge the sample. Finally, excess mounting media was removed with a tissue and the cover-slip was sealed on the edges using a transparent nail polish and allowed to dry before imaging.

2.5.2.3 Confocal imaging. The samples above were imaged using Zeiss LSM 880 confocal microscope using 10× (plan-apochromat/0.45 M27) and 20× (plan-apochromat/0.8 M27) objectives. Z-stacks of individual samples were acquired with tile-scanning for each optical section. Images were processed with Fiji[66] to derive maximum intensity projection of Z-stacks and to adjust contrast and brightness. Figures were put together at the highest possible resolution using Keynote (Apple Inc. Cupertino, California) and level functions were used on the digital images to make them consistent with visual observation. No quantitative image analysis was carried out on such a level adjusted image.

2.5.2.4 Survival analysis. 5 mL of 1% agarose solution was poured in fly vials and allowed to solidify. Vials were wiped thoroughly to remove excess water from the walls and a piece of

nonabsorbent cotton was placed inside each vial (ESI Fig. SI-9†) to avoid fly contact with agarose medium. In small feeding caps 250 μL of 1% PDA coated MSN, 1% PEG coated MSN, as-synthesized MSN, 100 mM glucose and only water samples in 1% low melting (LM) agarose were added with 0.8% amaranth FCF dye as an ingestion indicator. One cap each was fixed on the inside wall of a vial with double sided tape. 25 healthy female flies were mildly CO_2 anesthetized and added to each vial. All conditions were set in triplicates. The flies were allowed to revive and vials were kept at 25 °C. Number of surviving flies were counted and transferred to fresh vials with freshly prepared nanoparticles in 1 % LM agarose every 24 hours.

2.6 Statistical analysis

Data is represented as mean ± SD (Fig. 3). Statistical analysis was performed using GraphPad Prism 5 (GraphPad Software, USA). Non-parametric Kruskal–Wallis test was performed for *in vitro* release studies for estimating difference of RhB dye release from a dye loaded nanoparticle at different pH at a given time point. A *p*-value of <0.05 was assumed to indicate statistically significant dye release at different pH environments. Survival assay data was plotted using the Kaplan–Meier method and curves were compared using log-rank (Mantel–Cox) test (Fig. 6). See ESI Table SI-1† for detailed results of statistical analysis.

3 Results and discussion

3.1 Characterization of MSNs

A series of mesoporous silica nanoparticles (MSNs) were synthesized by changing the solvent mixture ratio to obtain particles of various sizes ranging from 200 nm to 900 nm. We chose particles with an average size of 650 ± 75 nm for ease of confocal microscopy imaging *in vivo* after feeding adult flies. As-synthesized MSN samples were then loaded with 0.005% RhB, and coated with PDA or PEG for 6 hours. All samples were characterized by DLS, SEM, TEM, FTIR and XPS. BET surface area analysis of as-synthesized MSNs show a surface area of ~482 $m^2\ g^{-1}$ and estimated pore diameter of 5.7 nm (see ESI Fig. SI-1A and B).† Since the MSNs were not calcined at higher temperatures after synthesis, a reduction in surface area could be attributed to incomplete evacuation of the template. However, since our primary goal was to observe delivery in *Drosophila* gut, partial presence of template and reduced loading capacity were not deterrents to our purpose. Surface coating by PDA or PEG was monitored by zeta (ζ) potential measurements which clearly show a shift in the net surface charge from around −26 mV for as-synthesized MSN particles (typical for MSNs)[11,67] to around −32 mV and −37 mV for PDA and PEG coated RhB@MSN particles respectively, confirming the alteration in surface properties of the synthesized MSNs by coating. Higher dispersibility of the coated samples also suggest a shift to higher negative charge of the particles. The average particle size of all the samples along with the ζ potential values are listed in Table 1.

In order to confirm the particle shape and size, scanning electron microscope (SEM) and transmission electron microscope (TEM) measurements were performed. SEM and TEM images clearly revealed spherical particles with a size of 635 ± 75 nm for the as-synthesized MSNs, 642 ± 60 nm for the PDA coated RhB@MSNs and 655 ± 55 nm for the PEG coated RhB@MSN samples (see Fig. 1, SI-3 and SI-4†). The difference between the coated and uncoated samples can be clearly seen from the TEM images (Fig. 1). The significant difference in particle diameter obtained by DLS when compared to TEM is attributed to agglomeration of the samples in water during DLS measurements. Although TEM images clearly show the difference in surface morphology for PDA or PEG coated samples when compared to the as-synthesized MSN particles, we performed XPS measurements in order to precisely establish the presence of PDA or PEG coating. Fig. 2 shows the XPS spectra for (i) as-synthesized MSN, (ii) PDA coated MSN and (iii) PEG coated MSN samples. As can be seen in Fig. 2A, all samples exhibit distinct peak at 103.5 eV,[68] characteristic of Si–O bonds. In case of the PDA coated MSN sample, the N 1s spectrum clearly shows

Table 1 Particle diameter and ζ potential values obtained from DLS measurements (also see Fig. SI-2). All samples were prepared in Milli-Q® water (pH ~ 8.0) and measured in duplicates

Measured parameters	As-synthesized MSNs	PDA coated RhB@MSN	PEG coated RhB@MSN
Particle diameter (nm)	819.5	945.48	962
Zeta potential (mV)	−26.63	−32.14	−37.02

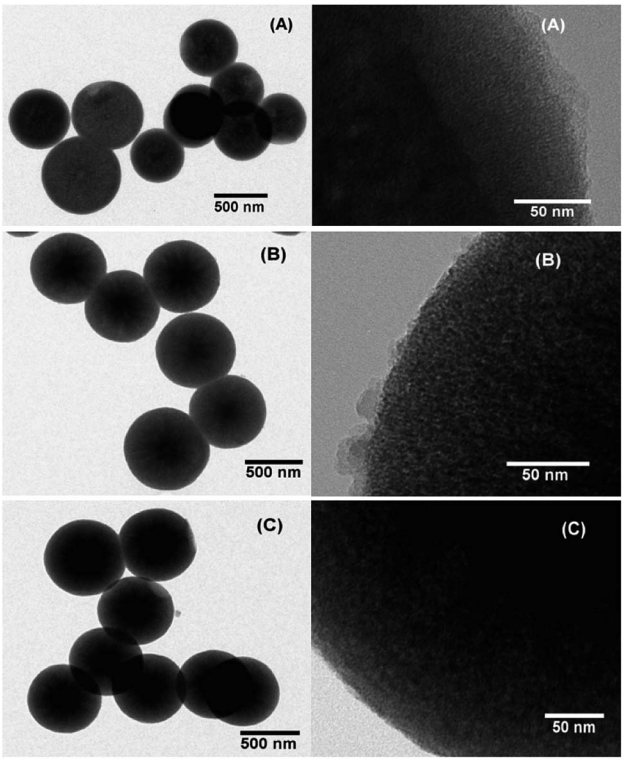

Fig. 1 TEM images of (A) as-synthesized MSN, (B) PDA coated RhB@MSN and (C) PEG coated RhB@MSN.

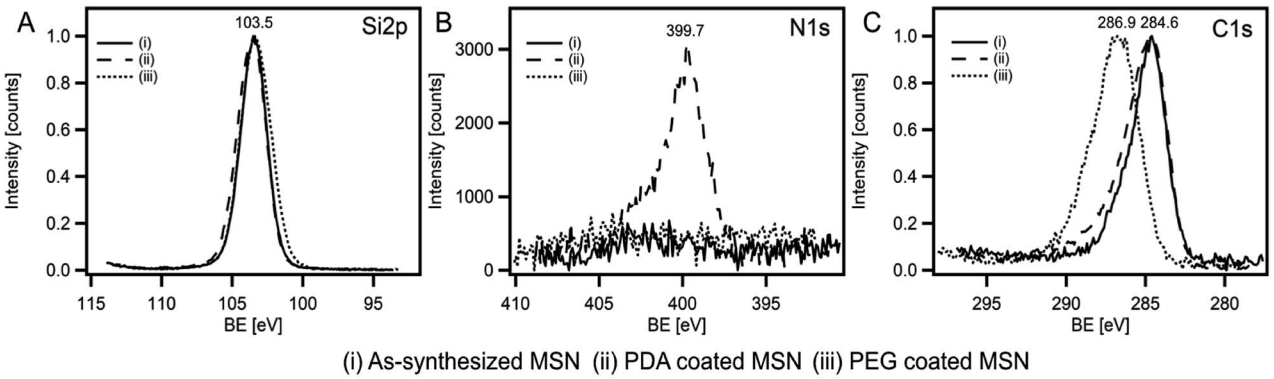

Fig. 2 (A) Intensity normalized Si 2p spectra of all three samples showing the distinct Si–O binding energy (BE) peak at 103.5 eV, (B) N 1s spectra of the same samples showing the distinct N–H peak at 399.7 eV for the PDA coated MSN sample and (C) intensity normalized C 1s spectra showing the formation of C–O bonds due to the presence of PEG on MSN surface.

the presence of N–H bond with a distinct peak at 399.7 eV confirming the presence of an amine group[35,69,70] on the MSN surface which is clearly absent for both PEG coated and as-synthesized MSN sample (Fig. 2B). Finally, in the case of PEG coated samples, C–O bonds in PEG results in a shift of the characteristic C–C peak from 284.6 eV to 286.8 eV (Fig. 2C) establishing the surface coupling of MSN by PEG.[71,72]

3.2 *In vitro* tests of the nanoparticles

In order to investigate the *in vitro* release of PDA and PEG coated RhB@MSNs, the synthesis optimized samples were suspended in three different pH (3.0, 7.4 and 9.0) solutions and RhB release was monitored hourly for 5 hours. We performed control measurements on uncoated RhB@MSN samples (Fig. 3A) as well. Clearly, both PDA and PEG coated samples show higher release at pH 3.0 as compared to pH 7.4 or 9.0 (Fig. 3B and C) and most RhB is released within two hours in both cases. To confirm the pH-triggered cargo release of both PDA and PEG in acidic pH, we performed ζ potential measurements of the samples under the same pH conditions. Control measurements on uncoated RhB@MSN and as-synthesized MSN samples were also performed. Table 2 summarizes the ζ potential for both PDA and PEG coated samples along with the uncoated MSN and as-synthesized MSNs at different pH.

As expected, all samples show positive potential at pH 3.0, suggesting protonation in acidic medium. Also, the particles are in an electrostatically stable configuration at pH 3.0 ($\geq$+30 mV) and pH 9.0 ($\leq$−30 mV) suggesting particle stability and less agglomeration in solution. The release profile in combination with ζ potential values for the uncoated RhB@MSN sample in pH 3.0 (Fig. 3A) reveals that there is decreased electrostatic interaction between the positively charged RhB and negatively charged silica surface in acidic medium[11] resulting in burst release of the dye within an hour. At neutral pH, the surface of uncoated RhB@MSN has a negative surface charge density resulting in further entrapment of RhB molecules in the MSN matrix and hence inhibiting its release. In the case of PDA coated RhB@MSN sample at pH 3.0 (Fig. 3B), the electrostatic interaction between the positively charged dye molecules and the protons in the acidic medium is reduced due to the presence of a polymeric barrier. As previously reported by DeMuth *et al.*,[11] and Casasús *et al.*,[73] the presence of a multilayer polyamine group on the surface of MSN would certainly inhibit the release of RhB molecules due to higher charge density. The

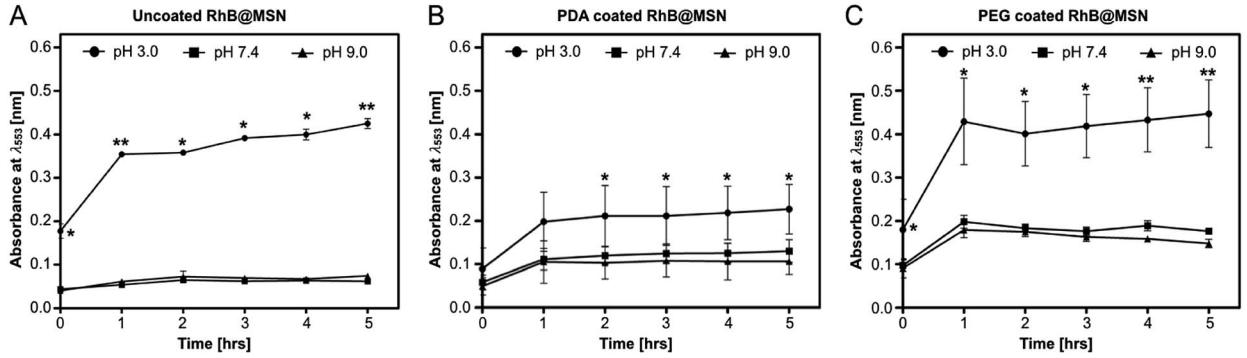

Fig. 3 *In vitro* release profile of dye cargo from (A) uncoated RhB@MSN, (B) PDA coated RhB@MSN and (C) PEG coated RhB@MSN showing release of RhB in acidic pH 3.0, neutral pH 7.4 and basic pH 9.0, hourly over a 5 hour period. Data is plotted as mean ± SD; $n = 4$; two replicates each from two different samples of each of the above nanoparticle species. For each time point, a non-parametric Kruskal–Wallis test was performed to determine if statistically significant differences exist in dye release at different pH. * indicates $p < 0.05$ and ** indicates $p < 0.01$.

Table 2 Zeta (ζ) potential measured for coated and uncoated MSN particles in different pH solutions. The values are a mean of two samples measured in duplicates

Samples	pH – 3.0	pH – 7.4	pH – 9.0
As-synthesized MSN	33.73	−25.2	−34.86
Uncoated RhB@MSN	34.45	−20.02	−36.19
PDA coated RhB@MSN	31.15	−26.31	−33.12
PEG coated RhB@MSN	29.42	−29.83	−39.33

polydopamine layer will expand due to the coulombic repulsion between the protonated amine groups causing it to expand in such a way that it reduces the effective pore diameter of the MSN and hence hinder the release of RhB from the pores.[11,73] Also, the PDA coated RhB@MSN sample has higher negative potential at neutral pH resulting in higher release of the dye when compared to uncoated RhB@MSN. However, when compared to the ζ potential value of the PEG coated RhB@MSN at pH 7.4, lower negative potential (−26 mV) suggests agglomeration of the particles in solution. In the case of PEG coated RhB@MSN at pH 3.0 (Fig. 3C) the total release of RhB is similar to that of the uncoated RhB@MSN (Fig. 3A). The increased total release of the dye molecules when compared to that of PDA coated RhB@MSN sample could be due to the hydrophilic nature of PEG. It is also possible that the use of low molecular weight PEG (PEG-400) would result in the formation of a thin layer of coating when compared to the PDA coated sample, resulting in more RhB release.[74] Finally at pH 9.0, all samples show negative potential ≤−30 mV suggesting that the particles are electrostatically stable in solution and hence less or no RhB release is observed. A schematic representation of the proposed mechanism of RhB release from the uncoated and coated RhB@MSN samples is shown in Fig. 4.

3.3 *In vivo* tests of the nanoparticles

To determine the pH responsive release and safety of synthesized MSNs coated with PDA and PEG in a whole organism model we chose adult *Drosophila melanogaster*. Almost all organ systems and cell types in the fly have been extensively studied in the context of development, cellular function and physiology.[75–77] Recently, flies are being increasingly used to study toxic impact of different classes of nanoparticles on cells, organs, physiology and ultimately survival and reproductive capacity of flies.[51,52,54–56,78–84] However, not many studies have focused on testing smart, stimulus responsive materials in flies to understand conserved mechanisms of nanocarrier based cargo/drug delivery. Only two recent studies have utilized the larval or adult fly gut for testing drug carrier materials.[58,60] The *Drosophila* gut is divided into three main regions: the foregut, midgut and the hindgut (Fig. 5A) with distinct acidic, neutral and alkaline zones like in mammals.[62,64] Ferguson *et al.*,[58] demonstrated recently in adult *Drosophila suzukii*, a pest species, that acidic pH-responsive poly(2-vinylpyridine)

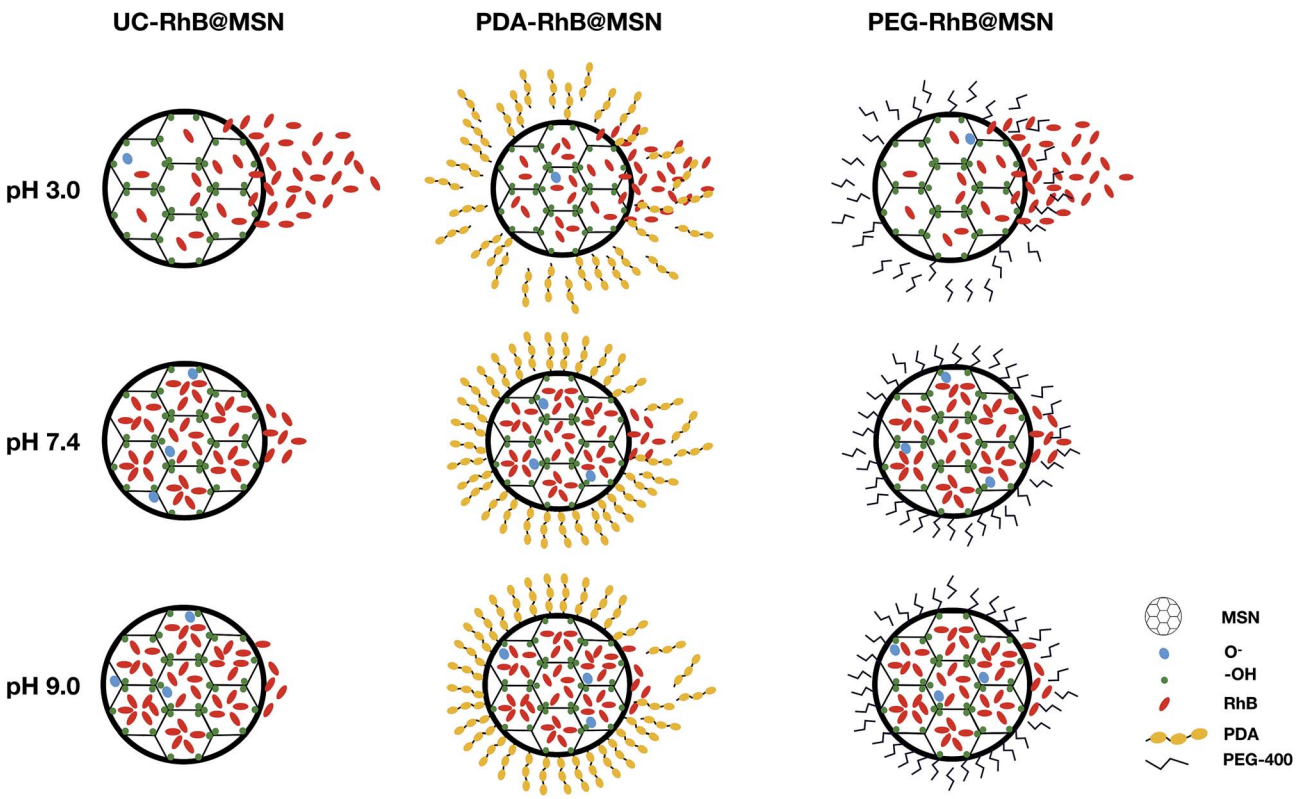

Fig. 4 Schematic representation of proposed *in vitro* RhB release mechanism for the uncoated and coated MSNs. Note: UC = uncoated.

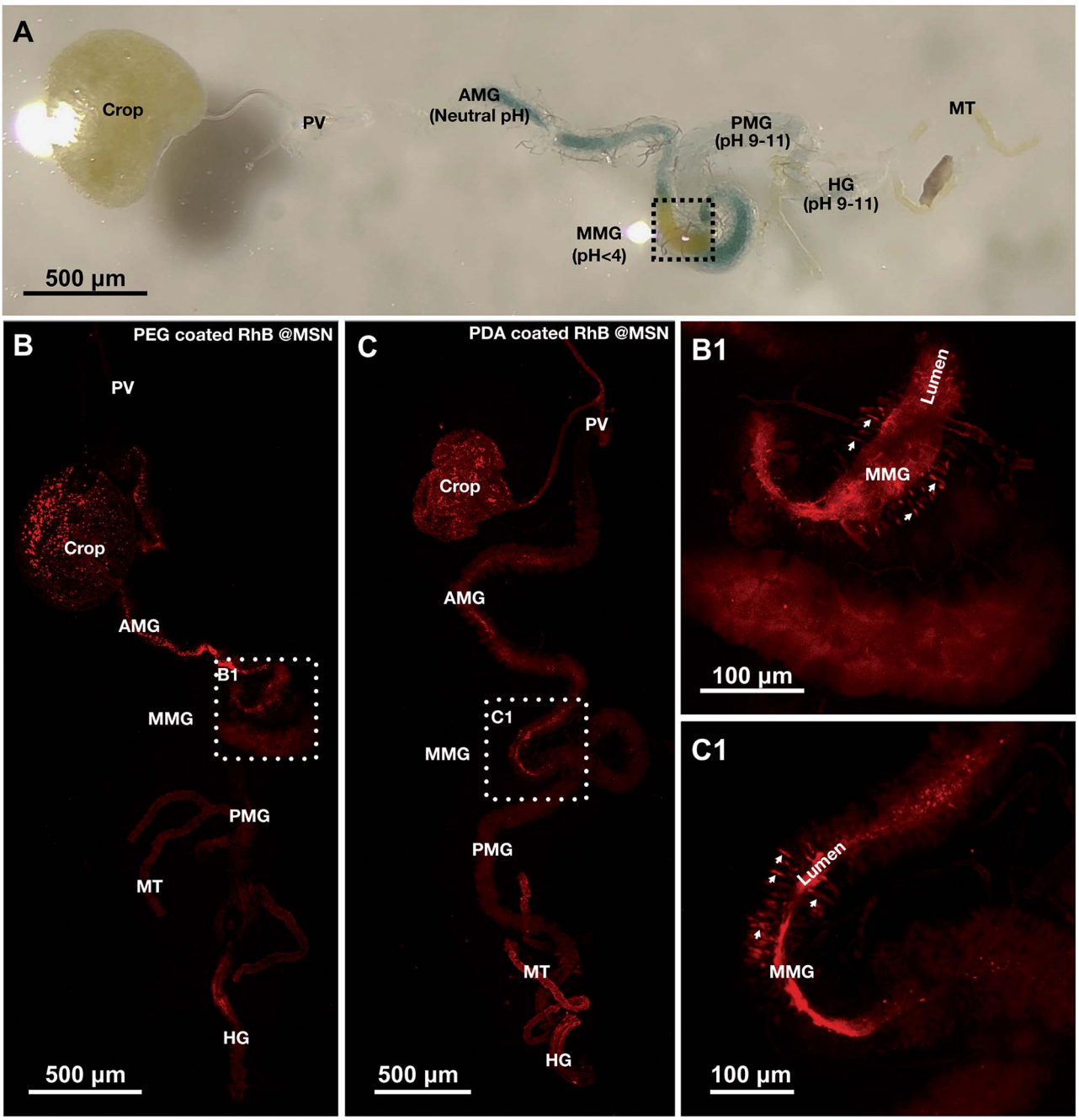

Fig. 5 (A) pH profile of a 4–5 days old CS-Q female fly gut fed with standard cornmeal medium with bromothymol blue for two hours after 24 h of starvation period, (B) *in vivo* particle distribution of 0.1 mg mL^{-1} PEG coated RhB@MSN and (C) 0.02 mg mL^{-1} PDA coated RhB@MSN fed CS-Q adult female. (B1) Middle midgut pH responsive release of PEG coated RhB@MSN and (C1) PDA coated RhB@MSN. Small white arrows in (B1 and C1) indicate paracellular transport of RhB in between the middle midgut (MMG) epithelial cells. Note: PV = proventriculus, AMG = anterior midgut, MMG = middle midgut, PMG = posterior midgut, MT = malpighian tubules and HG = hindgut.

microcapsules release their cargo in the fly midgut. To further test the feasibility of the fly gut as a model system for testing smart cargo release from biocompatible nanoparticles, we tested the pH-triggered release of our PDA and PEG coated MSNs and performed *in vivo* comparative study of the release, in the better characterized and genetically tractable *Drosophila melanogaster* species. As mentioned in the experimental section, 0.02 mg mL^{-1} of PDA and 0.1 mg mL^{-1} of PEG coated RhB@MSNs were fed to female flies and then they were kept for 30 minutes in a humid petri dish before dissection. The passage of these nanoparticles in the fly gut were visualized by confocal imaging of dissected guts. We observed that intact and discrete PEG coated RhB@MSN particles were present in the insect crop, where recently ingested food is stored before passing down through the midgut. Very low background fluorescence indicated that hardly any RhB@MSN particle rupture and RhB

release in the neutral pH of the crop (Fig. 5B). Discrete fluorescent signals from PEG coated RhB@MSN particles were also observed in the neutral pH of anterior midgut (AMG), in spite of saturated fluorescent signals due to particle accumulation, indicating that they were still intact at that zone (Fig. 5B). Remarkably, in the acidic middle midgut (MMG), with a pH < 4.0, discrete red fluorescent signal was lost and replaced by diffused red signal (area marked by white dotted box and inset in Fig. 5B and B1). This strongly suggests that, as *in vitro*, RhB release *in vivo* was in the MMG due to the highly acidic pH environment. Interestingly, the MMG also shows distinct red filamentous staining pattern, perpendicular to the gut lumen and spanning the gut walls. Based on previous studies of gut morphology,[64,85] we think these filamentous staining patterns are caused by paracellular (*i.e.*, in between the cells) transport of water soluble RhB dye, across the MMG epithelial cell layer (Fig. 5B1 and C1). Midguts of mammals and insects including flies, exhibit both transcellular transport (through the cells) and paracellular (in between cells) transport of small molecules, nutrients, drugs and insecticides.[61,86,87] Stressors like injury and cold temperature shock has been observed to induce such paracellular leakage of dyes in flies.[88,89] In our case, it is possible that the stress of food and water deprivation before nanoparticle feeding may result in the observed paracellular dye seepage from the MMG lumen. The preferred mode of transport across gut epithelium is likely influenced by the size, charge and orientation of the cargo molecule. A study in the lepidopteran larvae midgut epithelium with two insecticidal peptides reported preferential transcellular transport for a fluorescein isothiocyanate conjugated *Aedes aegypti* peptide trypsin modulating oostatic factor (FITC-Aea-TMOF) and paracellular transport of a Rhodamine labeled neuropeptide proctolin (Rh-proctolin).[90] We intend to conduct future studies to elucidate the role of nutrient deprivation states and the physicochemical properties of specific cargoes on transport across the fly gut epithelium.

The release of PDA coated RhB@MSN along the gut is similar to the PEG coated RhB@MSN in many respects and follows the same general pattern from crop to MMG (Fig. 5C and C1). The notable differences are (i) PDA coated RhB@MSN showed clumping all the way upto the MMG and (ii) higher background fluorescence in the crop and AMG. The more discrete nature of the PEG coated RhB@MSN compared to PDA coated RhB@MSN might be attributed to the higher electrostatic repulsion between individual particles due to higher negative surface charge at neutral pH of the former than the latter (Table 2). The higher background fluorescence of the PDA coated RhB@MSNs could be due to relatively higher levels (than the PEG coated RhB@MSNs preparation) of leftover un-encapsulated RhB in our preparation.

We also fed flies uncoated RhB@MSNs and looked at the release profile of RhB. In accordance with the *in vitro* release data (Fig. 3A), some RhB release and paracellular dye leakage in the epithelium was also observed in the acidic MMG (ESI Fig. SI-7B†). As explained in the previous section, this could be due to the fact that RhB is positively charged and could fit in an electrostatically stable configuration inside the negatively charged interior of the MSNs at neutral and alkaline pH. At acidic pH the decreased electrostatic interaction between the positively charged RhB and the silica surface results in a burst release of the dye molecule. However, a lot of discrete and also aggregated dye signals (very likely the particles themselves) are observed in the MMG and in the crop (ESI Fig. SI-7B†). The aggregation could due to the lower negative potential of the uncoated RhB@MSN (Table 2). The overall brighter signal seen in the image is in line with our observation that more dye is retained in uncoated RhB@MSN and that some RhB cargo is lost during the coating process of RhB@MSNs with PEG/PDA. Finally, feeding flies with free RhB as a control convincingly shows that RhB dye as possibly other cargo (the various dye loaded & coated/uncoated MSNs), is retained preferentially in the crop and then in the MMG (ESI Fig. SI-7A, A1, SI-7B and B1†) and also shows paracellular leak in between the MMG epithelial cells. Overall, our results suggest that coating with polymers could improve desirable properties of the cargo loaded MSNs. It reduces aggregation and potentially regulates cargo release from the MSNs. In other such applications, polymer coating increases longevity of systemically circulating nanoparticles and functionalize particles to be stimuli responsive.[24,91]

3.4 Survival analysis upon nanoparticle feeding

The quantification of survival was performed by placing the flies in vials with 1% agarose bed and small plastic feeding caps (see ESI Fig. SI-9†) loaded with different MSN species along with control samples. Flies were exposed to PDA/PEG coated and as-synthesized MSN particles in low melting (LM) agarose. Only 1% LM agarose (water) and 100 mM glucose in 1% LM agarose served as controls. A food grade indicator dye, Amaranth, was included in all samples to check for ingestion. Number of

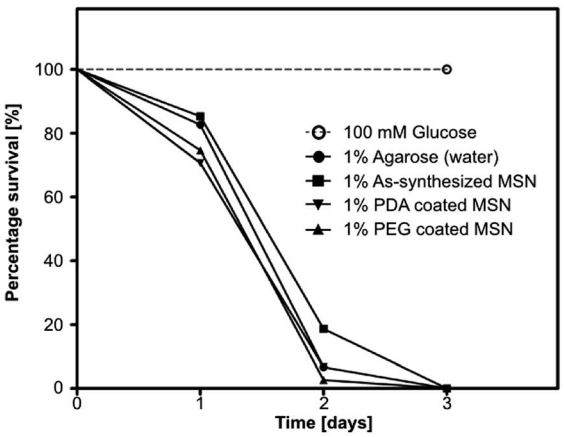

Fig. 6 Kaplan–Meier survival plots of young (0–4 days post eclosion) CS-Q female flies on 1% low melting (LM) agarose with 10 mg mL^{-1} as-synthesized MSN, PDA coated MSN and PEG coated MSN. Total 75 flies split in groups of 25 each were kept solely on the above nanoparticle species. Also shown are survival plots from similar number of flies kept on 100 mM glucose and water in 1% LM agarose. Log-rank (Mantel–Cox) test revealed no statistically significant difference between the group curves. 100 mM glucose control group is not included in the analysis as no flies died during the duration of the experiment.

surviving flies was recorded every 24 hours. All flies on the agarose (water) control failed to survive beyond 3 days due to lack of nutrition (Fig. 6). The nanoparticle fed flies followed the same trend for survival as that of the water control, suggesting that as-synthesized MSNs as well as PDA and PEG coated MSNs do not provide nutrition but were also likely non-toxic at 1% (10 mg mL^{-1}) concentration as they did not kill flies earlier than the water control.

4 Conclusions

In this work, we have compared pH-responsive release of RhB from mesoporous silica nanoparticles coated with two polymers: polydopamine (PDA) and polyethylene glycol (PEG) in the *Drosophila melanogaster* gut. We observe that both these types of carrier particles show specific release of RhB cargo in the highly acidic (pH < 4.0) middle midgut of flies. PEG coated particles show better release profile and clump less compared to the PDA coated species. Interestingly, uncoated RhB@MSNs also exhibit acid responsive cargo release like the coated MSNs. Our survival tests show that the various nanoparticles (coated and uncoated) are nontoxic at the conditions tested and are not a source of nutrition to flies. The use of *Drosophila melanogaster* to verify enteric pH responsive release provides an inexpensive and importantly, a genetic whole organism model to monitor drug release from a large range of functionalized materials. Most work on testing the long-term tissue or organ specific effects of the drug delivering nanoparticles are carried out on common laboratory rodents like mice and rats. Such studies require extensive animal experimentation clearance. In contrast we believe flies offer a rapid mode of carrying out similar studies, at a far lower cost and the ability to further explore the effect of nanoparticle exposure on specific molecular pathways, gene expression, physiology and behaviour. In addition to assessing the effect of the carrier material, it is not a long stretch to see that flies can easily be co-opted to study the biology of the cargo molecule interacting with their target cells/organs and also to monitor the systemic non-specific effect on cells and organs away from their delivery site as they circulate inside the organism over time.[57] The expeditious nature of such studies in flies will also allow faster fine tuning of the already-existing materials to function optimally. We also anticipate that cleverly designed functional materials can be used to uncover fundamental physiological, cellular, molecular mechanisms underlying proper gut function and its communication with other organs in flies.

Conflicts of interest

There are no conflicts to declare.

Acknowledgements

The authors acknowledge financial support from SIU and NCCS. We thank Dr B. L. V. Prasad, CSIR-National Chemical Laboratory, Pune, for fruitful discussions and feedback. We also thank Dr C. P. Vinod and the CMC facility at CSIR-National Chemical Laboratory, Pune, for help with XPS measurements. We thank Dr Amit Yadav for help with SEM facility use at NCMR, Pune. We thank the Sophisticated Analytical Instrument Facility (SAIF), IIT Bombay, for help with TEM measurements. We are grateful to NCCS imaging facility for assistance during long hours of imaging. Finally, we thank Dr Das and Dr Bajpe's research group members for feedback and support.

Notes and references

1 M. Bruneau, S. Bennici, J. Brendle, P. Dutournie, L. Limousy and S. Pluchon, *J. Controlled Release*, 2019, **294**, 355–371.
2 R. Amorim, N. Vilaça, O. Martinho, R. M. Reis, M. Sardo, J. Rocha, A. M. Fonseca, F. Baltazar and I. C. Neves, *J. Phys. Chem. C*, 2012, **116**, 25642–25650.
3 M. G. Rimoli, M. R. Rabaioli, D. Melisi, A. Curcio, S. Mondello, R. Mirabelli and E. Abignente, *J. Biomed. Mater. Res., Part A*, 2008, **87**, 156–164.
4 C. Orellana-Tavra, R. J. Marshall, E. F. Baxter, I. A. Lázaro, A. Tao, A. K. Cheetham, R. S. Forgan and D. Fairen-Jimenez, *J. Mater. Chem. B*, 2016, **4**, 7697–7707.
5 W. Cai, J. Wang, C. Chu, W. Chen, C. Wu and G. Liu, *Adv. Sci.*, 2019, **6**, 1801526.
6 P. Horcajada, C. Serre, G. Maurin, N. A. Ramsahye, F. Balas, M. Vallet-Regí, M. Sebban, F. Taulelle and G. Férey, *J. Am. Chem. Soc.*, 2008, **130**, 6774–6780.
7 P. Horcajada, C. Serre, M. Vallet-Regí, M. Sebban, F. Taulelle and G. Férey, *Angew. Chem., Int. Ed. Engl.*, 2006, **118**, 6120–6124.
8 Y. Guo, J. Wang, D. Zhang, T. Qi and G. L. Li, *Colloids Surf., A*, 2019, **561**, 1–8.
9 C.-Y. Sun, C. Qin, X.-L. Wang, G.-S. Yang, K.-Z. Shao, Y.-Q. Lan, Z.-M. Su, P. Huang, C.-G. Wang and E.-B. Wang, *Dalton Trans.*, 2012, **41**, 6906–6909.
10 G. Férey, *Chem. Soc. Rev.*, 2008, **37**, 191–214.
11 P. DeMuth, M. Hurley, C. Wu, S. Galanie, M. R. Zachariah and P. DeShong, *Microporous Mesoporous Mater.*, 2011, **141**, 128–134.
12 M. Sönmez, D. Ficai, A. Ficai, L. Alexandrescu, M. Georgescu, R. Trusca, D. Gurau, M. A. Titu and E. Andronescu, *Int. J. Pharm.*, 2018, **549**, 179–200.
13 X.-Y. Lou, Y.-P. Li and Y.-W. Yang, *Biotechnol. J.*, 2019, **14**, e1800354.
14 Y. Lu, Y. Yang, Z. Gu, J. Zhang, H. Song, G. Xiang and C. Yu, *Biomaterials*, 2018, **175**, 82–92.
15 B. G. Trewyn, I. I. Slowing, S. Giri, H.-T. Chen and V. S.-Y. Lin, *Acc. Chem. Res.*, 2007, **40**, 846–853.
16 B. G. Trewyn, S. Giri, I. I. Slowing and V. S.-Y. Lin, *Chem. Commun.*, 2007, **31**, 3236–3245.
17 J. Wen, K. Yang, F. Liu, H. Li, Y. Xu and S. Sun, *Chem. Soc. Rev.*, 2017, **46**, 6024–6045.
18 L. Yuan, Q. Tang, D. Yang, J. Z. Zhang, F. Zhang and J. Hu, *J. Phys. Chem. C*, 2011, **115**, 9926–9932.
19 S. Alberti, G. J. A. A. Soler-Illia and O. Azzaroni, *Chem. Commun.*, 2015, **51**, 6050–6075.

20 L. Tan, M.-Y. Yang, H.-X. Wu, Z.-W. Tang, J.-Y. Xiao, C.-J. Liu and R.-X. Zhuo, *ACS Appl. Mater. Interfaces*, 2015, **7**, 6310–6316.
21 L. Maggini, I. Cabrera, A. Ruiz-Carretero, E. A. Prasetyanto, E. Robinet and L. De Cola, *Nanoscale*, 2016, **8**, 7240–7247.
22 X. Li, C. Xie, H. Xia and Z. Wang, *Langmuir*, 2018, **34**, 9974–9981.
23 D. Chang, Y. Gao, L. Wang, G. Liu, Y. Chen, T. Wang, W. Tao, L. Mei, L. Huang and X. Zeng, *J. Colloid Interface Sci.*, 2016, **463**, 279–287.
24 J. S. Suk, Q. Xu, N. Kim, J. Hanes and L. M. Ensign, *Adv. Drug Delivery Rev.*, 2016, **99**, 28–51.
25 K. Yang, H. Luo, M. Zeng, Y. Jiang, J. Li and X. Fu, *ACS Appl. Mater. Interfaces*, 2015, **7**, 17399–17407.
26 G.-F. Luo, W.-H. Chen, Y. Liu, Q. Lei, R.-X. Zhuo and X.-Z. Zhang, *Sci. Rep.*, 2014, **4**, 6064.
27 Y. Hu, Z. Zhao, T. Harmon, P. R. Pentel, M. Ehrich and C. Zhang, *Biomaterials*, 2018, **182**, 72–81.
28 P. Laskar, J. Dey and S. K. Ghosh, *Colloids Surf., B*, 2016, **139**, 107–116.
29 S. Niedermayer, V. Weiss, A. Herrmann, A. Schmidt, S. Datz, K. Müller, E. Wagner, T. Bein and C. Bräuchle, *Nanoscale*, 2015, **7**, 7953–7964.
30 X. Zeng, G. Liu, W. Tao, Y. Ma, X. Zhang, F. He, J. Pan, L. Mei and G. Pan, *Adv. Funct. Mater.*, 2017, **27**, 1605985.
31 C. Liang, H. Wang, M. Zhang, W. Cheng, Z. Li, J. Nie, G. Liu, D. Lian, Z. Xie, L. Huang and X. Zeng, *J. Colloid Interface Sci.*, 2018, **525**, 1–10.
32 M. E. Lynge, R. van der Westen, A. Postma and B. Städler, *Nanoscale*, 2011, **3**, 4916–4928.
33 W. Cheng, J. Nie, N. Gao, G. Liu, W. Tao, X. Xiao, L. Jiang, Z. Liu, X. Zeng and L. Mei, *Adv. Funct. Mater.*, 2017, **27**, 1704135.
34 W. Cheng, C. Liang, L. Xu, G. Liu, N. Gao, W. Tao, L. Luo, Y. Zuo, X. Wang, X. Zhang, X. Zeng and L. Mei, *Small*, 2017, **13**, 1700623.
35 W. Cheng, J. Nie, L. Xu, C. Liang, Y. Peng, G. Liu, T. Wang, L. Mei, L. Huang and X. Zeng, *ACS Appl. Mater. Interfaces*, 2017, **9**, 18462–18473.
36 Y. Duo, Y. Li, C. Chen, B. Liu, X. Wang, X. Zeng and H. Chen, *RSC Adv.*, 2017, **7**, 39641–39650.
37 W. Cheng, X. Zeng, H. Chen, Z. Li, W. Zeng, L. Mei and Y. Zhao, *ACS Nano*, 2019, **13**, 8537–8565.
38 A.-K. Pada, D. Desai, K. Sun, N. Prakirth Govardhanam, K. Törnquist, J. Zhang and J. M. Rosenholm, *Int. J. Mol. Sci.*, 2019, **20**, 3408.
39 A. U. Kura, S. Fakurazi, M. Z. Hussein and P. Arulselvan, *Chem. Cent. J.*, 2014, **8**, 46.
40 V. Kumar, N. Sharma and S. S. Maitra, *Int. Nano Lett.*, 2017, **7**, 243–256.
41 A. H.-H. Wong, H. Li, Y. Jia, P.-I. Mak, R. P. d. S. Martins, Y. Liu, C. M. Vong, H. C. Wong, P. K. Wong, H. Wang, H. Sun and C.-X. Deng, *Sci. Rep.*, 2017, **7**, 9109.
42 J. L. Wilding and W. F. Bodmer, *Cancer Res.*, 2014, **74**, 2377–2384.
43 U. Schäfer and H. Jäckle, *Drosophila Melanogaster: A genetic tool, Comparative Genomics*, Springer, 2000, pp. 23–41.
44 B. H. Jennings, *Mater. Today*, 2011, **14**, 190–195.
45 S. E. Mohr, *First in Fly: Drosophila Research and Biological Discovery*, Harvard University Press, 2018.
46 U. B. Pandey and C. D. Nichols, *Pharmacol. Rev.*, 2011, **63**, 411–436.
47 L. T. Reiter, L. Potocki, S. Chien, M. Gribskov and E. Bier, *Genome Res.*, 2001, **11**, 1114–1125.
48 M. Allocca, S. Zola and P. Bellosta, *Drosophila melanogaster - Model for Recent Advances in Genetics and Therapeutics*, InTech, 2018.
49 B. Ugur, K. Chen and H. J. Bellen, *Dis. Models Mech.*, 2016, **9**, 235–244.
50 L. I. Held Jr, *Deep homology? Uncanny similarities humans and flies uncovered by Evo-Devo*, Cambridge University Press, 2019.
51 X. Liu, D. Vinson, D. Abt, R. H. Hurt and D. M. Rand, *Environ. Sci. Technol.*, 2009, **43**, 6357–6363.
52 R. Posgai, M. Ahamed, S. M. Hussain, J. J. Rowe and M. G. Nielsen, *Sci. Total Environ.*, 2009, **408**, 439–443.
53 M. Ahamed, R. Posgai, T. J. Gorey, M. Nielsen, S. M. Hussain and J. J. Rowe, *Toxicol. Appl. Pharmacol.*, 2010, **242**, 263–269.
54 M. Alaraby, B. Annangi, R. Marcos and A. Hernández, *J. Toxicol. Environ. Health, Part B*, 2016, **19**, 65–104.
55 B. Jovanović, V. J. Cvetković and T. L. Mitrović, *Chemosphere*, 2016, **144**, 43–49.
56 S. A. Pappus and M. Mishra, *Adv. Exp. Med. Biol.*, 2018, **1048**, 311–322.
57 F. Barandeh, P.-L. Nguyen, R. Kumar, G. J. Iacobucci, M. L. Kuznicki, A. Kosterman, E. J. Bergey, P. N. Prasad and S. Gunawardena, *PLoS One*, 2012, **7**, e29424.
58 C. T. J. Ferguson, A. A. Al-Khalaf, R. E. Isaac and O. J. Cayre, *PLoS One*, 2018, **13**, e0201294.
59 T. T. Su, *Wiley Interdiscip. Rev.: Dev. Biol.*, 2019, **8**, e346.
60 S. Jiang, C. P. Teng, W. C. Puah, M. Wasser, K. Y. Win and M.-Y. Han, *ACS Biomater. Sci. Eng.*, 2015, **1**, 1077–1084.
61 I. Miguel-Aliaga, H. Jasper and B. Lemaitre, *Genetics*, 2018, **210**, 357–396.
62 G. Overend, Y. Luo, L. Henderson, A. E. Douglas, S. A. Davies and J. A. T. Dow, *Sci. Rep.*, 2016, **6**, 27242.
63 M. Strand and C. A. Micchelli, *PLoS One*, 2013, **8**, e80608.
64 S. Shanbhag and S. Tripathi, *J. Exp. Biol.*, 2009, **212**, 1731–1744.
65 G. Chen, Z. Teng, X. Su, Y. Liu and G. Lu, *J. Biomed. Nanotechnol.*, 2015, **11**, 722–729.
66 J. Schindelin, I. Arganda-Carreras, E. Frise, V. Kaynig, M. Longair, T. Pietzsch, S. Preibisch, C. Rueden, S. Saalfeld, B. Schmid, J.-Y. Tinevez, D. J. White, V. Hartenstein, K. Eliceiri, P. Tomancak and A. Cardona, *Nat. Methods*, 2012, **9**, 676–682.
67 T. Ribeiro, E. Coutinho, A. S. Rodrigues, C. Baleizão and J. P. S. Farinha, *Nanoscale*, 2017, **9**, 13485–13494.
68 T. Gross, M. Ramm, H. Sonntag, W. Unger, H. M. Weijers and E. H. Adem, *Surf. Interface Anal.*, 1992, **18**, 59–64.
69 R. A. Zangmeister, T. A. Morris and M. J. Tarlov, *Langmuir*, 2013, **29**, 8619–8628.
70 W. Tamakloe, D. A. Agyeman, M. Park, J. Yang and Y.-M. Kang, *J. Mater. Chem. A*, 2019, **7**, 7396–7405.

71 V. B. Damodaran, C. J. Fee, T. Ruckh and K. C. Popat, *Langmuir*, 2010, **26**, 7299–7306.
72 K. C. Popat, S. Sharma and T. A. Desai, *J. Phys. Chem. B*, 2004, **108**, 5185–5188.
73 R. Casasús, E. Climent, M. D. Marcos, R. Martínez-Máñez, F. Sancenón, J. Soto, P. Amorós, J. Cano and E. Ruiz, *J. Am. Chem. Soc.*, 2008, **130**, 1903–1917.
74 S.-A. Yang, S. Choi, S. M. Jeon and J. Yu, *Sci. Rep.*, 2018, **8**, 185.
75 H. J. Bellen, C. Tong and H. Tsuda, *Nat. Rev. Neurosci.*, 2010, **11**, 514–522.
76 A. Singh and K. D. Irvine, *Dev. Dyn.*, 2012, **241**, 1–2.
77 Q. Liu and L. H. Jin, *Frontiers in Cell and Developmental Biology*, 2017, **5**, 29.
78 B.-H. Mao, Z.-Y. Chen, Y.-J. Wang and S.-J. Yan, *Sci. Rep.*, 2018, **8**, 2445.
79 V. Sundararajan, P. Dan, A. Kumar, G. D. Venkatasubbu, S. Ichihara, G. Ichihara and S. S. Mohideen, *Appl. Surf. Sci.*, 2019, **490**, 70–80.
80 D. J. Gorth, D. M. Rand and T. J. Webster, *Int. J. Nanomed.*, 2011, **6**, 343–350.
81 P. Dan, V. Sundararajan, H. Ganeshkumar, B. Gnanabarathi, A. K. Subramanian, G. D. Venkatasubu, S. Ichihara, G. Ichihara and S. Sheik Mohideen, *Appl. Surf. Sci.*, 2019, **484**, 568–577.
82 M. C. Chifiriuc, A. C. Ratiu, M. Popa and A. A. Ecovoiu, *Int. J. Mol. Sci.*, 2016, **17**, 36.
83 A. Raj, P. Shah and N. Agrawal, *Sci. Rep.*, 2017, **7**, 15617.
84 A. Raj, P. Shah and N. Agrawal, *PLoS One*, 2017, **12**, e0178051.
85 V. K. Dimitriadis, *J. Insect Physiol.*, 1991, **37**, 167–177.
86 S. Denecke, L. Swevers, V. Douris and J. Vontas, *Insect Biochem. Mol. Biol.*, 2018, **103**, 22–35.
87 W. H. Karasov, *J. Exp. Biol.*, 2017, **220**, 2495–2501.
88 H. A. MacMillan, G. Y. Yerushalmi, S. Jonusaite, S. P. Kelly and A. Donini, *Sci. Rep.*, 2017, **7**, 8807.
89 R. J. Katzenberger, S. Chtarbanova, S. A. Rimkus, J. A. Fischer, G. Kaur, J. M. Seppala, L. C. Swanson, J. E. Zajac, B. Ganetzky and D. A. Wassarman, *Elife*, 2015, **4**, e04790.
90 L. Fiandra, M. Casartelli, G. Cermenati, N. Burlini and B. Giordana, *J. Insect Physiol.*, 2009, **55**, 10–18.
91 M. A. C. Stuart, W. T. S. Huck, J. Genzer, M. Müller, C. Ober, M. Stamm, G. B. Sukhorukov, I. Szleifer, V. V. Tsukruk, M. Urban, F. Winnik, S. Zauscher, I. Luzinov and S. Minko, *Nat. Mater.*, 2010, **9**, 101–113.

